



Mo(II) complexes of 8-aminoquinoline and their immobilization in MCM-41



Marta S. Saraiva^a, Carla D. Nunes^a, Teresa G. Nunes^b, Maria José Calhorda^{a,*}

^a Departamento de Química e Bioquímica, CQB, Faculdade de Ciências da Universidade de Lisboa, Campo Grande, Ed. C8, 1749-016 Lisboa, Portugal

^b Centro de Química Estrutural, Instituto Superior Técnico, Universidade Técnica de Lisboa, Av. Rovisco Pais, 1049-001 Lisboa, Portugal

ARTICLE INFO

Article history:

Received 7 August 2012

Received in revised form 18 January 2013

Accepted 31 January 2013

Available online 15 February 2013

Keywords:

Molybdenum

MCM

Oxidation catalysis

8-Aminoquinoline

Alkenes

ABSTRACT

Two new Mo(II) complexes [MoBr(η^3 -C₃H₅)(CO)₂(**8-aq**)] (**1**) and [Mo₂(CO)₃(**8-aq**)] (**2**) containing the bidentate 8-aminoquinoline ligand (**8-aq**) were synthesized and characterized. They were immobilized in MCM-41. A 3-iodopropyltrimethoxysilane spacer reacted both with the surface, through the silane, and through the other end, with the coordinated **8-aq** of complexes **1** and **2**, leading to an immobilized form of the complex (**MCM-Pr-1,2**). In an alternative route, **8-aq** reacted with 3-iodopropyltrimethoxysilane to form a new ligand **L₁**, which could be supported in the MCM-41 and then react with the metal precursors to afford (**MCM-L₁-1,2**). The complexes and the materials were characterized using FTIR and NMR spectroscopies, and the structure of the materials was checked with powder X-ray diffraction and nitrogen adsorption isotherms. The first synthetic procedure was less efficient in terms of metal load inside the channels of the materials.

The complexes and the new materials were tested as catalytic precursors in the epoxidation of *cis*-cyclooctene, styrene, 1-octene, *R*-(+)-limonene, geraniol, *cis*-3-hexene-1-ol and *trans*-2-hexene-1-ol, using *tert*-butylhydroperoxide (TBHP) as oxidant. Although almost all the catalysts were 100% selective toward the epoxide, the conversions were in general poor. The best catalyst was complex **1**, but the conversions dropped after immobilization. Conversions could be a bit improved by a careful choice of reaction conditions, the most effective being the absence of added solvent (the substrate acted as solvent).

© 2013 Elsevier B.V. All rights reserved.

1. Introduction

The development of heterogeneous catalysts remains a very important research field, since it has not yet been possible to combine in the same system the advantages of heterogeneous catalysts, such as the easy catalyst recovery, with those of homogeneous ones, namely the selectivity. Several routes to prepare new heterogeneous systems have been designed in the last decades [1,2]. Using a selected material to act as support where active catalysts can be grafted counts as one of the most successful ones, in special owing to the family of the Mobil MCM family of mesoporous solids, reported for the first time in 1992 [3,4]. These materials containing organized hexagonal channels with a diameter of ~2–50 nm can be easily functionalized by reaction of the silanol groups in the walls with molecules carrying Si(OR)₃ substituents. The fourth position around silicon can range from an organometallic complex, to a ligand which can bind a number of metal fragments, to a special active molecule. The formation of

a covalent bond between the wall of the material and the catalyst or catalyst precursor helps, on one hand, to prevent leaching, allowing the reutilization of the catalyst; on the other, it is possible to vary the immobilized catalyst in a relatively easy way, so that small active homogeneous catalysts can be supported with minimal change, and their catalytic properties are not likely to change [5–8]. These functionalized inorganic materials have been widely applied in several fields, such as catalysis and optoelectronics [1,5,9–11].

The Mo(II) complexes [Mo(η^3 -C₃H₅)Br(CO)₂(CH₃CN)₂] [12,13] and [Mo₂(CO)₃(CH₃CN)₂] [14] have also proved to be very versatile, since the nitrile ligands are easily substituted by other ligands. They have been used as catalysts [15], in particular in allylic alkylations [16], imine aziridation, [17] or phosphine oxidation [18]. It has also been shown that [Mo(η^3 -C₃H₅)X(CO)₂(N–N)] (X = Cl, Br) species can behave selectively as catalyst precursors in olefin epoxidation when *t*-butyl hydroperoxide (TBHP) is the oxidant, [19] a reactivity previously detected in other Mo(II) complexes, namely [Mo(η^5 -C₅H₅)(CO)₃(CH₃)] [20]. Mo(II) complexes are initially oxidized to active Mo(VI) species. Catalysts containing Mo(VI) are used in the ARCO-Halcon process for homogeneous olefin epoxidation with TBHP as oxidant, thus contributing to the renewed interest in molybdenum chemistry [21]. Chiral molybdenum complexes in

* Corresponding author. Tel.: +351 217500196; fax: +351 217500088.

E-mail addresses: mssaraiva@fc.ul.pt (M.S. Saraiva), cmnunes@fc.ul.pt (C.D. Nunes), teresa.nunes@ist.utl.pt (T.G. Nunes), mjc@fc.ul.pt (M.J. Calhorda).

MCM-41 have also been developed for asymmetric oxidation catalysis [22,23].

We have used $[\text{Mo}(\eta^3\text{-C}_3\text{H}_5)\text{Br}(\text{CO})_2(\text{CH}_3\text{CN})_2]$ and $[\text{Mo}_2(\text{CO})_3(\text{CH}_3\text{CN})_2]$ complexes as precursors for catalytic olefin epoxidation with TBHP, using a variety of N–N (bidentate nitrogen ligands) in homogeneous conditions or immobilized in different supports, from MCM-41, to clays, or silsesquioxanes, but it is not yet totally clear why the activity of some systems increases with immobilization for some ligands, but not for others [7,19,24–30].

In this work, we study the reactivity of another bidentate dinitrogen ligand, 8-aminoquinoline (**8aq**), bound to Mo(II) in the two families of complexes, and explored several routes to support the heterogeneous counterparts in MCM 41. This ligand has been associated with several metal centers to catalyze carbonylation and other reactions [31].

2. Experimental

2.1. Catalysts preparation

All reagents were obtained from Aldrich and used as received. Commercial grade solvents were dried and deoxygenated by standard procedures (diethyl ether, tetrahydrofuran and toluene over sodium/benzophenone ketyl; dichloromethane, dimethylformamide over calcium hydride and methanol over magnesium), distilled under nitrogen, and kept over 4 Å molecular sieves. Complexes $[\text{Mo}(\eta^3\text{-C}_3\text{H}_5)\text{Br}(\text{CO})_2(\text{CH}_3\text{CN})_2]$ [12,13], $[\text{Mo}(\eta^3\text{-C}_3\text{H}_5)\text{Br}(\text{CO})_2(\text{L})]$ [24], $[\text{Mo}_2(\text{CO})_3(\text{CH}_3\text{CN})_2]$ [14], and $[\text{Mo}_2(\text{CO})_3(\text{L})]$ [25] were prepared according to literature methods.

The complex $[\text{Mo}(\eta^3\text{-C}_3\text{H}_5)\text{Br}(\text{CO})_2(\mathbf{8}\text{-aq})]$ (**1**) was prepared by adding a solution of 8-aminoquinoline (**8aq**) (1.2 mmol, 0.173 g) in dichloromethane to a stirred solution of $[\text{Mo}(\eta^3\text{-C}_3\text{H}_5)\text{Br}(\text{CO})_2(\text{CH}_3\text{CN})_2]$ (1 mmol, 0.355 g) in dichloromethane in inert atmosphere and allowed to stir for 2 h. The orange solid was filtered, washed with diethyl ether, and dried under vacuum during 3 h (325 mg, 78% yield).

$[\text{Mo}_2(\text{CO})_3(\mathbf{8}\text{-aq})]$ (**2**) was prepared by adding a solution of 8-aminoquinoline (**8aq**) (1.2 mmol, 0.173 g) in methanol to a stirred solution of $[\text{Mo}_2(\text{CO})_3(\text{CH}_3\text{CN})_2]$ (1 mmol, 0.488 g) also in methanol, in inert atmosphere, and allowing to stir overnight. The solution was concentrated by removing part of the solvent, and diethyl ether was added. The brown solid formed was filtered, washed with diethyl ether, and dried under vacuum during 3 h (480 mg, 83% yield).

The modified 8-aminoquinoline ligand (**L**₁) was obtained from the reaction between 3-iodopropyltrimethoxysilane (1.0 mmol, 0.196 mL) and a solution of **8aq** (1.0 mmol, 0.144 g) in 30 mL of tetrahydrofuran, after stirring at 339 K during 72 h. The solution turned orange without formation of any precipitate, and an oil was formed after removing the solvent (303 mg, yield 70%).

MCM-41 and derivatized materials were synthesized by adopting a methodology previously described, using $[(\text{C}_{14}\text{H}_{33})\text{N}(\text{CH}_3)_3]\text{Br}$ as template [8]. Template extraction from MCM-41 was performed by refluxing the materials with HCl acidified methanol instead of a calcination procedure. Prior to the grafting experiment, physisorbed water and methanol were removed by heating at 453 K in vacuum (10^{-2} Pa) for 2 h. Two batches of MCM-41 were prepared for use in each of the pathways as will be discussed later.

(3-Iodopropyl)trimethylsilyl-MCM-41 (**MCM-Pr**) resulted from the addition of 2.0 mL of 3-iodopropyltrimethoxysilane to a suspension of 1 g of **MCM-41** in 30 mL of toluene, and reflux for 24 h. The yellow suspension was filtered, washed with 4 × 20 mL dichloromethane, and dried under vacuum during 3 h.

Further functionalization of MCM-41 with molybdenum(II) fragments was carried out by the reaction of 1.0 g of **MCM-Pr** with a solution of complex **1** (1.0 mmol, 0.417 g) or complex **2** (1.0 mmol, 0.578 g) in dimethylformamide and triethylamine (1.5 mmol, 0.207 g) at 273 K. The mixture was stirred for 72 h at room temperature. The suspension was filtered, washed with 4 × 20 mL dichloromethane, and dried under vacuum during 3 h. **MCM-Pr-1** and **MCM-Pr-2** were obtained, respectively.

An alternative functionalization was achieved by grafting the **L**₁ ligand in MCM-41. A solution of **L**₁ ligand (5.0 mmol, 2.17 g) in toluene was added to a suspension of 1 g of **MCM-41** (**1**) in 30 mL of toluene, and allowed to reflux for 24 h. The yellow suspension of **MCM-L**₁ was filtered, washed with 4 × 20 mL dichloromethane, and dried under vacuum during 3 h.

A suspension of this immobilized **MCM-L**₁ ligand (1.0 g) in dichloromethane could then react with $[\text{MoBr}(\eta^3\text{-C}_3\text{H}_5)(\text{CO})_2(\text{CH}_3\text{CN})_2]$ (1.0 mmol, 0.355 g) in dichloromethane. The mixture was stirred overnight, filtered, washed with dichloromethane, and dried under vacuum during 3 h, to yield **MCM-L**₁-**1**. **MCM-L**₁-**2** was obtained by a similar reaction with $[\text{Mo}_2(\text{CO})_3(\text{CH}_3\text{CN})_2]$ (1.0 mmol, 0.488 g), using methanol as solvent.

2.2. Catalysts characterization

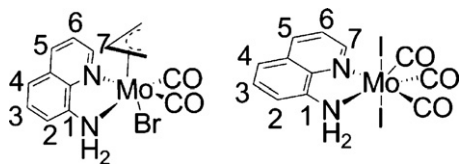
FTIR spectra were obtained as KBr pellets (complexes) and Diffuse Reflectance (DRIFT) measurements (materials) on a Nicolet 6700 in the 400–4000 cm^{-1} range with 4 cm^{-1} resolution.

Microanalyses for C, H, N, and Mo quantification were performed at CACTI, University of Vigo (C, H, and N analyses on a Fisons EA 1108, and Mo on a Perkin Elmer Optima 4300DV using In as internal standard).

¹H and ¹³C solution NMR spectra were obtained with a Bruker Avance 400 spectrometer. Solid state ²⁹Si and ¹³C NMR measurements were performed at room temperature on a Bruker MSL 300P spectrometer operating at 59.60 and 75.47 MHz for the observation of ²⁹Si and ¹³C resonances, respectively. The standard magic angle spinning (MAS) cross polarization–dipolar decoupling RF pulse sequence (CP–DD) was used under about 4 kHz spinning rate. For the acquisition of ²⁹Si spectra, 5 ms contact time was chosen, 6 s recycling delay, and a number of scans always higher than 3000 were selected; the Hartmann–Hahn condition was optimized using tetrakis-trimethylsilylsilane and tetramethylsilane (TMS) was the external reference to set the chemical shift scale. ¹³C spectra were recorded with 2 ms contact time, 4 s recycling delay and a number of scans higher than 900. The Hartmann–Hahn condition was optimized using glycine, also the external reference to set the chemical shift scale (¹³CO at 176.1 ppm).

Powder XRD measurements were taken on a Philips Analytical PW 3050/60 X'Pert PRO (theta/2 theta) equipped with X'Celerator detector and with automatic data acquisition (X'Pert Data Collector (v2.0b) software), using a monochromatized Cu-Kα radiation as incident beam, 40 kV – 30 mA.

N₂ sorption measurements were obtained in an automatic apparatus (ASAP 2010; Micromeritics). BET specific surface areas (*S*_{BET}, *p/p*⁰ from 0.03 to 0.13) and specific total pore volume, *V*_p were estimated from N₂ adsorption isotherms measured at 77 K. The pore size distributions (PSD) were calculated by the BJH method using the modified Kelvin equation with correction for the statistical film thickness on the pore walls [32,33]. The statistical film thickness was calculated using Harkins–Jura equation in the *p/p*⁰ range from 0.1 to 0.95. Prior to the measurements, samples were degassed and physisorbed water was removed by heating at 723 K for MCM and 413 K for the derivatized materials (to minimize the destruction of the functionalities) in vacuum for 2 h 30 m. TGA studies were



Scheme 1. Structure and atom numbering scheme of complexes $[\text{MoBr}(\eta^3\text{-C}_3\text{H}_5)(\text{CO})_2(\mathbf{8}\text{-aq})]$ (**1**, left) and $[\text{MoI}_2(\text{CO})_3(\mathbf{8}\text{-aq})]$ (**2**, right).

performed using a Perkin-Elmer TGA7 thermobalance system at a heating rate of $10\text{ }^\circ\text{C min}^{-1}$ under N_2 .

2.3. Catalytic tests

Complexes and materials were tested as catalysts in the epoxidation of *cis*-cyclooctene, styrene, 1-octene, *R*(+)-limonene, geraniol, *cis*-3-hexene-1-ol and *trans*-2-hexene-1-ol, using *tert*-butylhydroperoxide (TBHP) as oxidant. The catalytic oxidation tests were carried out at 328 K under normal atmosphere in a reaction vessel equipped with a magnetic stirrer and a condenser. In a typical experiment, the vessel was loaded with olefin (100%), internal standard (DBE), catalyst (1%), oxidant (200%), and 3 mL of solvent. Addition of the oxidant determines the initial time of the reaction. The course of the reactions was monitored by quantitative GC-analysis by collecting samples at 10 min, 30 min, 1 h, 1 h 30 min, 2, 4, 6, 8, and 24 h of reaction. These samples were treated as described previously prior to injection in the GC column [25].

2.4. Epoxidation of *cis*-cyclooctene, styrene, 1-octene, *R*(+)-limonene, geraniol, *cis*-3-hexen-1-ol, and *trans*-2-hexen-1-ol

Epoxidation of *cis*-cyclooctene, styrene, 1-octene, *R*(+)-limonene, geraniol, *cis*-3-hexen-1-ol, and *trans*-2-hexen-1-ol

Substrate (800 mg: 7.3 mmol of *cis*-cyclooctene, 7.7 mmol of styrene, 7.1 mmol of 1-octene, 5.87 mmol of *R*(+)-limonene, 5.2 mmol of geraniol; 7.99 mmol of *cis*-3-hexen-1-ol and *trans*-2-hexen-1-ol), 800 mg dibutyl ether (internal standard), 1 mol % of catalyst, 2.65 mL of TBHP (5.5 M in *n*-decane) and 3 mL of CH_2Cl_2 .

3. Results and discussion

3.1. Characterization of catalysts

The new complexes (Scheme 1) $[\text{MoBr}(\eta^3\text{-C}_3\text{H}_5)(\text{CO})_2(\mathbf{8}\text{-aq})]$ (**1**; **8-aq** = 8-aminoquinoline) and $[\text{MoI}_2(\text{CO})_3(\mathbf{8}\text{-aq})]$ (**2**) were

characterized by FTIR, ^1H and ^{13}C NMR spectroscopy and elemental analysis.

The $\nu(\text{C}=\text{O})$ bands were observed in the FTIR spectra at 1958, 1928, and 1832 cm^{-1} in $[\text{MoBr}(\eta^3\text{-C}_3\text{H}_5)(\text{CO})_2(\mathbf{8}\text{-aq})]$ (**1**) and at 2068, 2016, 1923, and 1869 cm^{-1} in $[\text{MoI}_2(\text{CO})_3(\mathbf{8}\text{-aq})]$ (**2**). The number of bands indicates that several isomers were formed [34,35]. Bands characteristic of the **8-aq** ligand appear at 1624 cm^{-1} in **1** and **2**, $\nu(\text{C}=\text{N})$, and at 1505 or 1508 cm^{-1} , $\nu\text{C}=\text{C}$ (**1** and **2**, respectively).

The spectra ^1H and ^{13}C NMR spectra (Table 2) show the peaks assigned to the protons and carbons of the **8-aq** ligand shifted from their positions in the free **8-aq** ligand, and those of the allyl ligand of **1**, confirming the coordination to Mo in complexes **1** and **2**. Elemental analysis (Table 1, Section 2.2) confirms the proposed structure shown in Scheme 1.

The organometallic derivatized materials were obtained by grafting a spacer (3-iodopropyltrimethoxysilane, **Pr**) in MCM and allowing it to react with complexes **1** and **2** containing coordinated **8aq** (route A), or by synthesizing the new ligand **L₁**, by modifying **8aq** through reaction with **Pr**, which then reacts with the precursors $[\text{MoBr}(\eta^3\text{-C}_3\text{H}_5)(\text{CO})_2(\text{CH}_3\text{CN})_2]$ or $[\text{MoI}_2(\text{CO})_3(\text{CH}_3\text{CN})_2]$ (route B). A third alternative, based on grafting complexes $[\text{MoBr}(\eta^3\text{-C}_3\text{H}_5)(\text{CO})_2(\mathbf{L}_1)]$ or $[\text{MoI}_2(\text{CO})_3(\mathbf{L}_1)]$ led to metal poor materials. Scheme 2 depicts the steps leading to the desired materials. It should be mentioned that the same Mo containing materials are obtained from both routes: **MCM-Pr-1** is the same as **MCM-L₁-1**, and **MCM-Pr-2** is the same as **MCM-L₁-2**. **Pr** and **L₁** identify the spacer grafted in MCM and thus also the synthetic pathway.

Two batches of the pure siliceous matrix MCM-41 (**MCM**) parent material, obtained by a template approach, were afterwards derivatized according to the pathways outlined in Scheme 2 [6]. In pathway A (Scheme 2, top), 3-iodopropyltrimethoxysilane is first grafted in the inner walls of pristine **MCM**, leading to **MCM-Pr**. Then it reacts with a solution of $[\text{Mo}(\eta^3\text{-C}_3\text{H}_5)\text{Br}(\text{CO})_2(\mathbf{8}\text{-aq})]$ (**1**) or $[\text{MoI}_2(\text{CO})_3(\mathbf{8}\text{-aq})]$ (**2**) in tetrahydrofuran at 339 K during 72 h, to afford the final materials **MCM-Pr-1** and **MCM-Pr-2**, containing 0.98 (0.1 mmol g^{-1}) and 0.68 wt% (0.07 mmol g^{-1}) of Mo, respectively.

Pathway B (Scheme 2, bottom) starts by grafting the **MCM** parent material with the ligand (**L₁**, inset in Scheme 2) synthesized by reaction of 3-iodopropyltrimethoxysilane with **8aq** in tetrahydrofuran at 339 K for 72 h. The resulting **MCM-L₁** material reacted with complexes $[\text{MoBr}(\eta^3\text{-C}_3\text{H}_5)(\text{CO})_2(\text{CH}_3\text{CN})_2]$ or $[\text{MoI}_2(\text{CO})_3(\text{CH}_3\text{CN})_2]$ to yield the organometallic materials **MCM-L₁-1** and **MCM-L₁-2**, respectively. The Mo load in these materials was found to be 4.85 (0.5 mmol g^{-1}) for **MCM-L₁-1** and 2.95 wt% (0.3 mmol g^{-1}) for

Table 1
Elemental analysis and relevant vibrational frequencies for $[\text{Mo}(\eta^3\text{-C}_3\text{H}_5)\text{Br}(\text{CO})_2(\mathbf{8}\text{-aq})]$ (**1**), $[\text{MoI}_2(\text{CO})_3(\mathbf{8}\text{-aq})]$ (**2**), **L₁**, and materials **MCM-Pr**, **MCM-Pr-1**, **MCM-Pr-2**, **MCM-L₁**, **MCM-L₁-1**, and **MCM-L₁-2**.

	Elemental analysis (%)				IR frequencies		
	C	H	N	Mo	$\nu_{\text{C}=\text{O}}$	$\nu_{\text{C}=\text{N}}$	$\nu_{\text{N}-\text{H}}$
1 ^a	39.29 (40.31)	3.08 (3.14)	6.62 (6.72)	^b	1958, 1928, 1832	1624	3203,3161
2 ^c	26.00 (25.81)	2.00 (1.91)	5.38 (4.92)	^b	2068, 2016, 1923	1624	3420, 3220
L₁ ^d	41.12 (41.48)	4.90 (5.34)	6.07 (6.45)	–	–	1616	3374, 3202
MCM-Pr	4.50 ^e	0.95 ^e	–	–	–	–	–
MCM-Pr-1	18.02	4.46	6.31	0.98(0.1) ^f	1920, 1824	1655, 1570	3452
MCM-Pr-2	16.70	4.07	5.90	0.68(0.07) ^f	1987, 1891, 1863	1655, 1571	3434
MCM-L₁	21.92 ^g	2.84 ^g	3.01	–	–	1638, 1578	3429
MCM-L₁-1	17.04	2.12	2.66	4.85(0.5) ^f	1942, 1852	1638, 1566	3409
MCM-L₁-2	18.00	2.70	2.30	2.95(0.3) ^f	1950, 1830	1635, 1560	3441

^a $\text{C}_{14}\text{H}_{13}\text{MoN}_2\text{O}_2\text{Br}$: found (calc.)

^b Not determined.

^c $\text{C}_{12}\text{H}_8\text{MoN}_2\text{I}_2$: found (calc.)

^d $\text{C}_{15}\text{H}_{23}\text{O}_3\text{N}_2\text{ISi}$: found (calc.)

^e Organic loading 0.6 mmol g^{-1}

^f Mo loading mmol g^{-1} .

^g Organic loading 1.0 mmol g^{-1} .

Table 2¹H and ¹³C NMR chemical shifts of free **8-aq**, [MoBr(η³-C₃H₅)(CO)₂(**8-aq**)] (**1**) and [Mo₂(CO)₃(**8-aq**)] (**2**) complexes.

	H ₂	H ₃	H ₄	H ₅	H ₆	H ₇	NH	Allyl ^a		
8-aq	6.93	7.31–7.37	7.15	8.05	7.31–7.37	8.75	4.98	–		
1	8.1	7.6	8.0	7.7	7.9	8.7	9.8	1.16/3.57/4.23		
2	8.65	7.79	7.71	7.71	7.94	9.04	n.o.	–		
	C ₁	C ₂	C ₃	C ₄	C ₅	C ₆	C ₇	C ₈	C ₉	Allyl ^a
8-aq	144.0	110.0	127.4	116.0	136.0	121.3	147.4	138.4	128.8	–
1	141.0	127.0	128.0	122.5	131.0	124.0	140.0	146.0	129.0	54.2/55.8/73.7
2	140.2	141.5	130.9	123.8	129.3	128.3	149.9	147.0	131.6	–

^a Most abundant isomer.

MCM-L₁-2. These results indicate that although both pathways lead to the same final materials, pathway B is more efficient as higher amounts of Mo are introduced in the parent **MCM**.

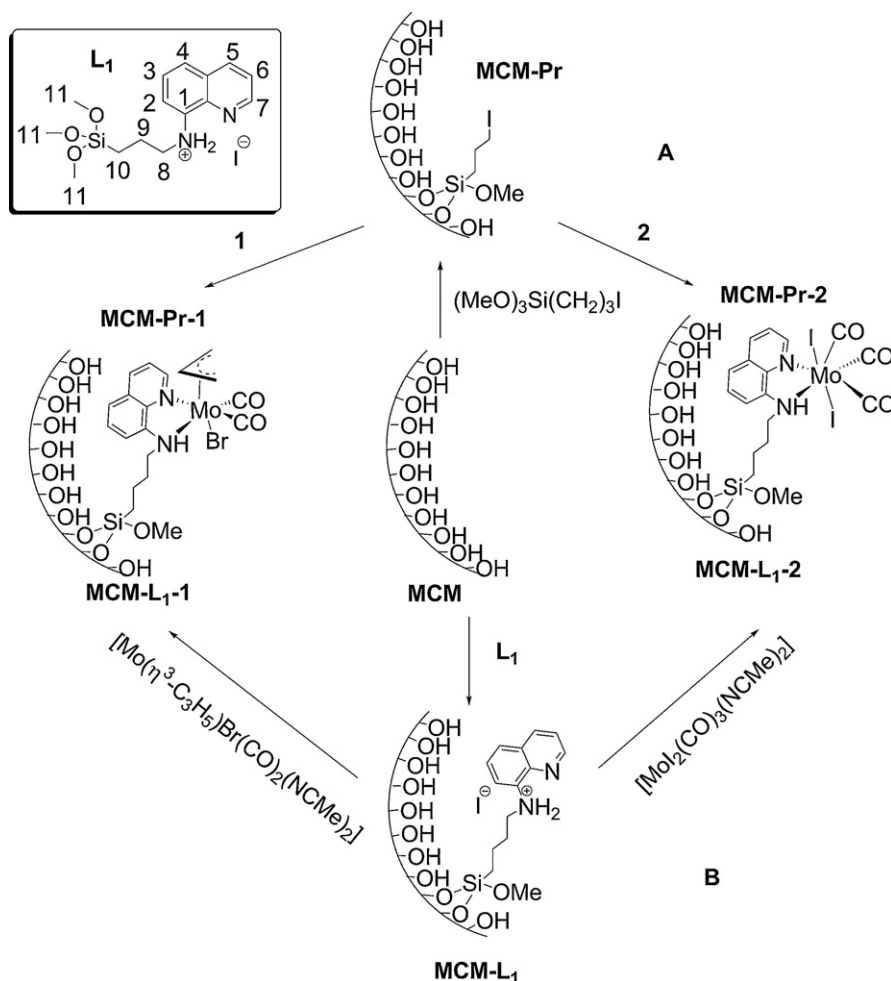
The C and N contents indicated a loading of 1 mmol g⁻¹ in **MCM-L₁**, based on the C/N ratio of 7.28. The analysis obtained after introduction of molybdenum indicate Mo loadings of 0.5 mmol g⁻¹ for **MCM-L₁-1** and 0.3 mmol g⁻¹ for **MCM-L₁-2**, respectively (C/N ratios 8.04 for **1** and 7.83 for **2**). This means that the metal precursor did not react with all the available **L₁** ligands. However, more molybdenum is immobilized in this way than following the alternative route leading to **MCM-Pr-1** and **MCM-Pr-2**, containing only 0.1 mmol g⁻¹ and 0.07 mmol g⁻¹ of Mo.

The powder XRD patterns of **MCM-Pr-1** and **MCM-L₁-1** are given in Fig. 1 (those of **MCM-Pr-2** and **MCM-L₁-2** are not shown). The pattern of the parent, calcined **MCM** material, shows four

reflections in the 2° < 2θ < 10° range, indexed to a hexagonal cell as (1 0 0), (1 1 0), (2 0 0), and (2 1 0). The *d* value of the (100) reflection is 37.9 Å, corresponding to a lattice constant of *a* = 44.3 Å (=2*d*₁₀₀/√3).

The observed peak intensity reduction is common to all materials and is even more significant in the materials with Mo. This is not due to a crystallinity loss, but rather to an X-ray scattering contrast reduction between the silica walls and pore-filling material. This has been observed for other types of materials and is well described in the literature [36–38]. The relevant textural properties of all materials are collected in Table 3.

Nitrogen adsorption studies at 77 K revealed that the pristine **MCM** sample exhibits a reversible type IV isotherm (Fig. 2), characteristic of mesoporous solids (pore width between 2 and 50 nm, according to IUPAC) [39]. The calculated textural parameters (*S*_{BET} and *V*_p) of this material agree with literature data (Table 2)

**Scheme 2.** Structure of ligand **L₁** and reaction scheme for preparation of heterogeneous catalysts.

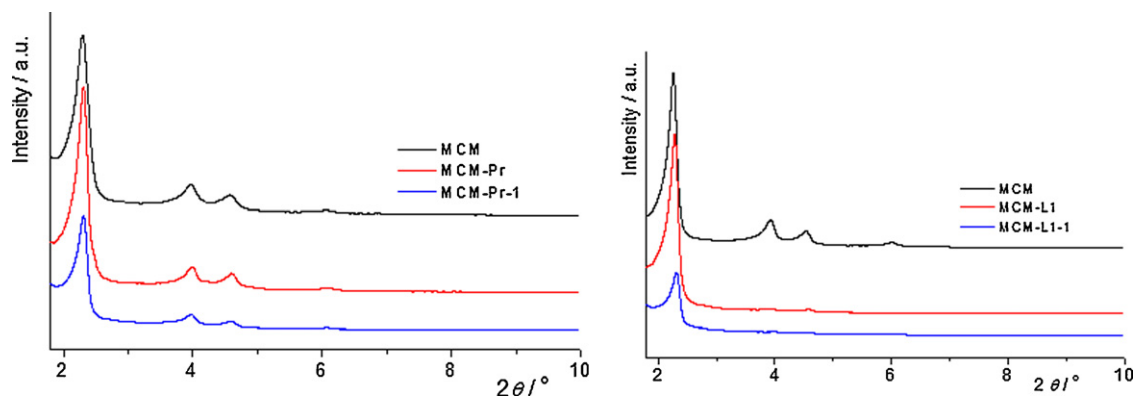


Fig. 1. XRD powder patterns of mesoporous materials **MCM-Pr**, **MCM-Pr**, **MCM-Pr-1**, **MCM-L1**, and **MCM-L1-1** prepared from pathway A (left) and B (right).

Table 3

Textural parameters for MCM host and derivatized materials from N₂ isotherms at 77 K and powder XRD data.

Sample	$d_{100}/\text{\AA}$	$a/\text{\AA}$	$S_{\text{BET}}/\text{m}^2 \text{g}^{-1}$	$\Delta S_{\text{BET}}^{\text{a}}/\%$	$V_{\text{p}}/\text{cm}^3 \text{g}^{-1}$	$\Delta V_{\text{p}}^{\text{b}}/\%$	$d_{\text{BJH}} \text{ (nm)}$
MCM	37.9	44.3	1040	–	0.920	–	3.50
MCM-Pr	38.6	44.0	886	–15	0.729	–21	3.36
MCM-Pr-1	38.6	44.0	801	–23	0.640	–30	3.36
MCM-Pr-2	38.6	44.3	887	–15	0.725	–21	3.28
MCM	39.1	45.0	1036	–	0.914	–	3.45
MCM-L1	40.3	44.4	450	–57	0.260	–72	2.67
MCM-L1-1	39.4	43.8	124	–88	0.112	–88	2.68
MCM-L1-2	39.0	44.4	115	–89	0.095	–90	2.67

^a Surface area variation relative to parent MCM.

^b Total pore volume variation relative to parent MCM.

[40,41]. The capillary condensation/evaporation steps appear in the 0.20–0.40 relative pressure range, and the sharpness of this step reflects the uniform pore size.

For the first set of materials in Table 3 (synthetic pathway A), the isotherm of the functionalized material **MCM-Pr** reveals much lower N₂ uptake, accounting for a decrease in V_{p} (21%) and a concomitant variation in S_{BET} (15%) compared to the parent **MCM**. This trend is observed after introduction of complex **1**, but there is no change when going from **MCM-Pr** to **MCM-Pr-2** suggesting that the amount of complex **2** introduced in the material must be very small, as determined from elemental analysis.

For the second set of materials (pathway B), the isotherm of the functionalized material **MCM-L1** reveals much lower N₂ uptake than in **MCM-Pr** accounting for a large decrease in V_{p} (72%) and a concomitant variation in S_{BET} (57%). Introduction of the precursor complexes inside the pores induces a further decrease of both V_{p} and S_{BET} (88–90%), in agreement with the decrease of the p/p° coordinates of the inflection points of the isotherms after post-synthesis treatments [42]. The height of the capillary condensation steps,

which is related to the volume of pore space confined by adsorbate film on the pore walls, is smaller in the case of the modified materials (Fig. 2). Furthermore, the maxima of the PSD curves determined by the BJH method, d_{BJH} , decrease concomitantly (Table 3).

Fig. 3 shows the thermogravimetric analyses (TGA) of the materials involved in pathway B in (Scheme 2). All materials experience mass losses corresponding to physisorbed water until 398 K, and start to decompose at higher temperatures.

The **MCM-L1** material displays a degradation process occurring between 398 and 1073 K, with loss of 21.1% weight, corresponding to a 0.85 mmol g^{–1} of the ligand inside the MCM pores. This value is in agreement with the total amount of **L1** (1 mmol g^{–1}) obtained from elemental analysis.

MCM-L1-1 and **MCM-L1-2** undergo loss of the organometallic moiety between 398 and 1073 K, corresponding to ca. 26.5%, or 0.6 mmol_{M₀} g^{–1} (**MCM-L1-1**) and ca. 23.3%, or 0.4 mmol_{M₀} g^{–1} (**MCM-L1-2**). These values agree quite well with those from elemental analysis, namely 0.5 mmol_{M₀} g^{–1} (**MCM-L1-1**) and 0.3 mmol_{M₀} g^{–1} (**MCM-L1-2**) respectively.

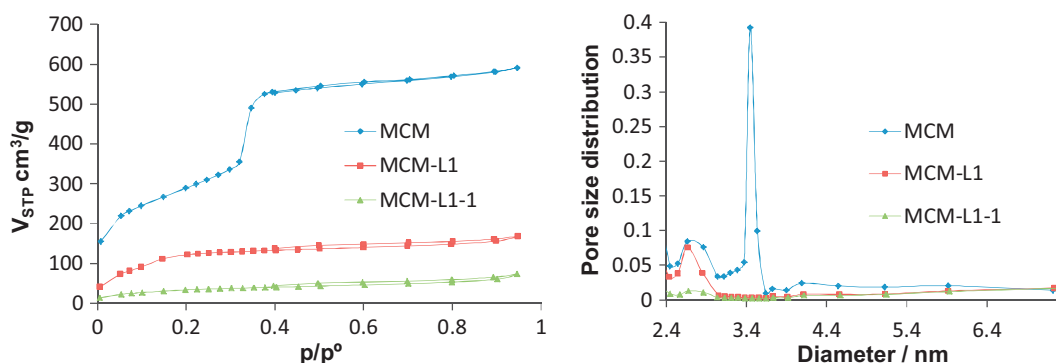


Fig. 2. Nitrogen adsorption isotherms of materials **MCM**, **MCM-L1**, and **MCM-L1-1** at 77 K (left); pore size distribution of **MCM**, **MCM-L1**, and **MCM-L1-1** (right).

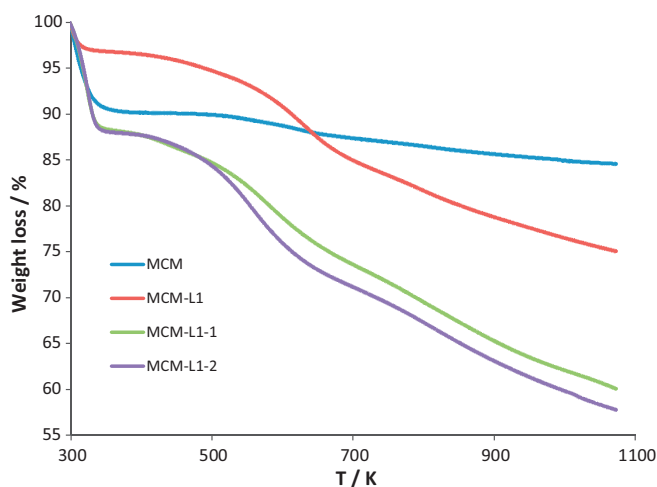


Fig. 3. TGA profiles of **MCM**, **MCM-L1**, **MCM-L1-1** and **MCM-L1-2**.

Similar profiles are obtained for materials **MCM-Pr-1** and **MCM-Pr-2**. After the release of physisorbed water before 398 K (TGA curves not shown), weight losses of $0.11 \text{ mmol}_{\text{Mo}} \text{ g}^{-1}$ and $0.08 \text{ mmol}_{\text{Mo}} \text{ g}^{-1}$, respectively, were found, comparable to $0.10 \text{ mmol}_{\text{Mo}} \text{ g}^{-1}$ (**MCM-Pr-1**) and $0.07 \text{ mmol}_{\text{Mo}} \text{ g}^{-1}$ (**MCM-Pr-2**) obtained from elemental analysis.

The presence of the immobilized $[\text{MoBr}(\eta^3\text{-C}_3\text{H}_5)(\text{CO})_2(\text{L}_1)]$ and $[\text{Mo}_2(\text{CO})_3(\text{L}_1)]$ complexes in the materials was probed by FTIR spectroscopy.

In the material **MCM-Pr** containing grafted 3-iodopropyltrimethoxysilane (**Pr**), the stretching vibrations modes of the mesoporous framework (Si–O–Si) are observed at around 1243, 1079, 956 cm^{-1} , as in the parent **MCM**, while the new bands at ca. 2982 and 2853 cm^{-1} are assigned to the $\nu(\text{C–H})$ stretching modes of the aliphatic propyl chain. The introduction of complexes **1** and **2** is confirmed by the presence of $\nu(\text{C}\equiv\text{O})$ stretching modes observed at 1920 and 1824 cm^{-1} for **MCM-Pr-1**, and 1987 , 1891 and 1863 cm^{-1} for **MCM-Pr-2**. These bands are slightly shifted from their position in the complexes, as the **L**₁ ligand differs from **8aq**, and they are broader. The observation of $\nu(\text{C=N})$ modes at 1654 and 1570 cm^{-1} (**MCM-Pr-1**) and at 1655 and 1571 cm^{-1} (**MCM-Pr-2**) further confirms the coordination of the metal fragments to the material.

When following pathway B, the **L**₁ ligand is grafted in **MCM**. Its presence is attested by the new bands at 2945 and 2850 cm^{-1} , assigned to the $\nu(\text{C–H})$ stretching of the aliphatic linear chain and aromatic C–H of the ring, as well as $\nu(\text{C=N})$ modes at 1638 and 1578 cm^{-1} . The strong stretching vibrational modes of the mesoporous framework (Si–O–Si) of **MCM-L**₁ are observed at ca. 1236 , 1080 , and 955 cm^{-1} , as in the parent **MCM**. The reaction with the precursor complexes $[\text{MoBr}(\eta^3\text{-C}_3\text{H}_5)(\text{CO})_2(\text{CH}_3\text{CN})_2]$ and $[\text{Mo}_2(\text{CO})_3(\text{CH}_3\text{CN})_2]$ leads to new $\nu(\text{C}\equiv\text{O})$ bands at 1942 and 1852 cm^{-1} (**MCM-L**₁-1), and at 1950 and 1830 cm^{-1} (**MCM-L**₁-2), slightly shifted from the values in the free complexes.

The materials were also characterized by ^{13}C CP MAS-DD and ^{29}Si CP MAS-DD solid state NMR.

As an example, the ^{13}C CP MAS-DD spectrum of **MCM-L**₁ presents the resonances of the propyl chain at 8.9 (Si–CH₂), 22.5 (CH₂–CH₂–CH₂) and 73.3 (HN–CH₂), and four signals at 121.8 , 130.7 , 146.8 and 176.0 ppm corresponding to aromatic carbons from the **L**₁ ligand. After reaction with $[\text{MoBr}(\eta^3\text{-C}_3\text{H}_5)(\text{CO})_2(\text{CH}_3\text{CN})_2]$, the resulting **MCM-L**₁-1 shows the three resonances of the propyl chain protons slightly shifted, at 8.4 (Si–CH₂), 23.0 (CH₂–CH₂–CH₂) and 72.6 (HN–CH₂), as well as the carbon resonances at 123.1 , 129.2 , 142.9 , 176.2 ppm (Fig. 4). In the material **MCM-L**₁-2, obtained from the reaction with

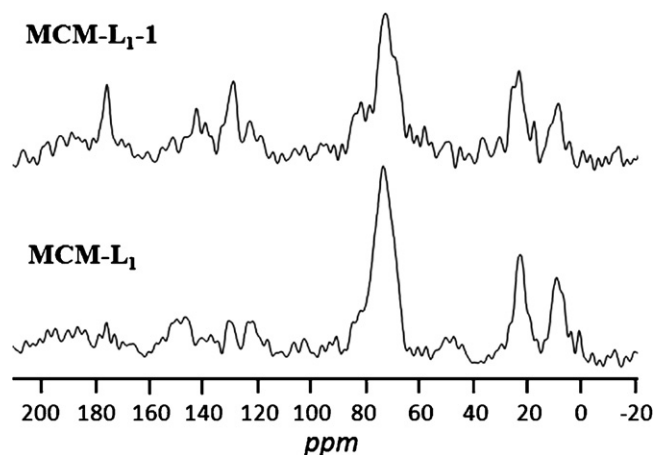


Fig. 4. ^{13}C CP MAS-DD spectra of **MCM-L**₁ (bottom) and **MCM-L**₁-1 (top).

$[\text{Mo}_2(\text{CO})_3(\text{CH}_3\text{CN})_2]$, those proton signals are observed at 9.2 (Si–CH₂), 22.9 (CH₂–CH₂–CH₂) and 73.4 (HN–CH₂), and the carbons at 123.4 , 129.8 , 143.0 and 173.8 ppm .

The ^{29}Si CP MAS-DD NMR spectrum of pristine **MCM**, displays three resonances at -109.2 , -100.6 and -91.4 ppm , characteristic of Q⁴, Q³ and Q² species of the silica framework, respectively (Fig. 5).

In **MCM-L**₁, the relative size of the Q⁴, Q³ and Q² signals changes, as both Q³ and Q² species disappear owing to the reaction with **L**₁. At the same time three broad signals at -65.0 , -55.0 and -51.5 ppm , assigned to T³, T² and T¹ organosilica species, appear in the spectrum. Introduction of the organometallic fragments $[\text{MoBr}(\eta^3\text{-C}_3\text{H}_5)(\text{CO})_2(\text{CH}_3\text{CN})_2]$ and $[\text{Mo}_2(\text{CO})_3(\text{CH}_3\text{CN})_2]$ does not significantly change the ^{29}Si CP MAS-DD NMR spectra, besides a slight shift of the signals, as the reaction occurs with the immobilized **L**₁ and should not involve the material walls.

3.2. Catalytic studies

3.2.1. Oxidation of substrates

Both complexes, $[\text{MoBr}(\eta^3\text{-C}_3\text{H}_5)(\text{CO})_2(\mathbf{8}\text{-aq})]$ (**1**) and $[\text{Mo}_2(\text{CO})_3(\mathbf{8}\text{-aq})]$ (**2**), and the final materials, **MCM-Pr-1**, **MCM-Pr-2**, **MCM-L**₁-1 and **MCM-L**₁-2, were tested as catalyst precursors

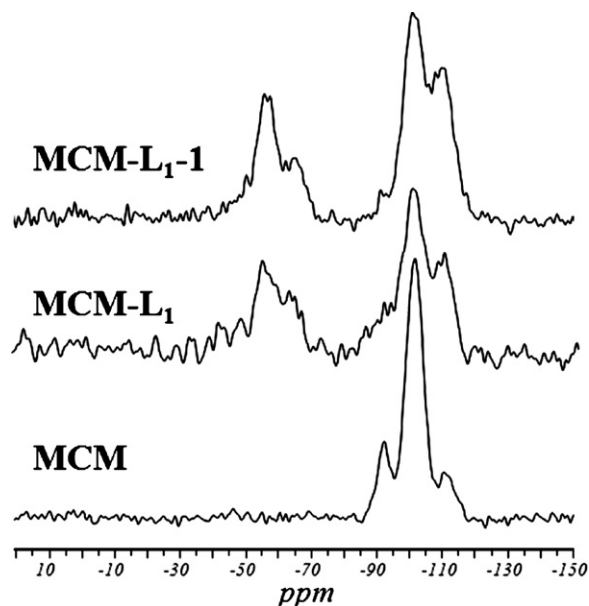


Fig. 5. ^{29}Si CP MAS-DD spectra of **MCM** (bottom), **MCM-L**₁ (center) and **MCM-L**₁-1 (top).

Table 4
Olefin oxidation catalyzed by $[\text{Mo}(\eta^3\text{-C}_3\text{H}_5)\text{Br}(\text{CO})_2]$ (**1**), $[\text{Mo}_2(\text{CO})_3]$ (**2**), **MCM-Pr-1**, **MCM-Pr-2**, **MCM-L₁-1** and **MCM-L₁-2**.

Entry	Epoxide ^a	Catalyst	Conversion ^{b,c} (%)	Selectivity ^{c,d} (%)
1		1	74	100
2		2	55	100
3		MCM-Pr-1	53	100
4		MCM-Pr-2	45	100
5		MCM-L₁-1	48	100
6		MCM-L₁-2	26	100
7		1	92 (86)	63 (84)
8		2	38 (14)	3 (54)
9		MCM-Pr-1	17 (22)	56 (34)
10		MCM-Pr-2	18 (4)	21 (34)
11		MCM-L₁-1	94 (81)	64 (76)
12		MCM-L₁-2	99 (14)	17 (60)
13		1	5	90
14		2	11	11
15		MCM-Pr-1	4	46
16		MCM-Pr-2	2	32
17		MCM-L₁-1	5	8
18		MCM-L₁-2	2	53
19		1	69	100
20		2	92	96
21		MCM-Pr-1	75	100
22		MCM-Pr-2	34	80
23		MCM-L₁-1	30	100
24		MCM-L₁-2	28	70
25		1	58	100
26		2	45	100
27		MCM-Pr-1	14	100
28		MCM-Pr-2	14	100
29		MCM-L₁-1	4	100
30		MCM-L₁-2	6	100
31		1	60	50
32		2	17	73
33		MCM-Pr-1	25	82
34		MCM-Pr-2	19	61
35		MCM-L₁-1	25	83
36		MCM-L₁-2	28	82
37		1	94	73 ^e
38		2	96	53 ^e
39		MCM-Pr-1	82	37 ^e
40		MCM-Pr-2	68	87 ^e
41		MCM-L₁-1	79	62 ^f
42		MCM-L₁-2	51	73 ^f

^a All reactions carried out in CH_2Cl_2 in the presence of 200 mol% oxidant (TBHP) and 1 mol% of molybdenum catalyst at 328 K.

^b Calculated after 24 h.

^c Values in parentheses refer to 8 h reaction time.

^d Calculated as "Yield of Epoxide"/"Conversion" \times 100% after 24 h.

^e 6,7-Epoxide formed as by-product.

^f 6,7-Epoxide and geraniol formed as by-products.

for olefin epoxidation using a set of substrates (*cis*-cyclooctene, styrene, 1-octene, *R*(+)-limonene, geraniol, *trans*-hex-2-en-1-ol, *cis*-hex-3-en-1-ol), and *tert*-butyl hydroperoxide (TBHP in decane) as oxygen donor, in dichloromethane, at 328 K (Table 4, see details in Section 2). No reaction took place in the absence of a catalyst.

All the tested catalysts oxidized *cis*-cyclooctene 100% selectively to the epoxide. The catalysts containing $\text{MoBr}(\eta^3\text{-C}_3\text{H}_5)(\text{CO})_2$ (**1**, **MCM-Pr-1** and **MCM-L₁-1**) show the highest conversions and homogeneous catalysts lead to higher conversions than heterogeneous ones.

The oxidation of styrene leads to the epoxide and benzaldehyde, this one arising from oxidative cleavage of the epoxide [30], and conversions are relatively low. The catalysts with the allyl ligand (**1**, **MCM-Pr-1** and **MCM-L₁-1**) have higher selectivity toward formation of the epoxide, while the others lead almost exclusively to substrate over-oxidation yielding benzaldehyde. Indeed, the amount of epoxide formed after 8 h is larger than after 24 h (Table 4,

entries 8, 10 and 12). The choice of catalyst and reaction time may thus determine the nature of the product.

Oxidation of 1-octene was carried out very inefficiently with all the catalysts (Table 4, entries 13–18), 11% being the highest conversion observed for complex **2** (entry 14). The highest selectivity toward the epoxide was observed with complex **1** as catalyst (entry 13), following the trend described for *cis*-cyclooctene and styrene.

The epoxidation of *trans*-hex-2-en-1-ol is promoted by all catalysts with fair to good substrate conversion. Catalysts **1**, **MCM-Pr-1** and **MCM-L₁-1** were completely selective to the epoxide (Table 2, entries 19, 21 and 23), while **2**, **MCM-Pr-2** and **MCM-L₁-2** yielded epoxides with lower selectivity and conversions (Table 4, entries 20, 22, 24).

Cis-hex-3-en-1-ol is selectively oxidized to the epoxide (100% for all catalysts), but the conversions are very low for the heterogeneous catalysts (4–14%). Only the homogeneous catalysts **1** and **2** show fair substrate conversions of 58% and 45%, respectively.

Table 5
Olefin oxidation catalyzed by $[\text{Mo}(\eta^3\text{-C}_3\text{H}_5)\text{Br}(\text{CO})_2(\mathbf{8}\text{-aq})]$ (**1**) changing solvent and temperature.

Entry	Epoxide	Solvent	Temperature (K)	Conversion ^{a,b} (%)	Selectivity ^{b,c} (%)
1	cis-Cyclooctene	CH ₂ Cl ₂	328	74	100
2		–	358	100 (6 h)	100
3		–	393	100 (10 min)	100
4	1-Octene	CH ₂ Cl ₂	328	5	90
5		CH ₃ CN	358	30	87
6		Toluene	393	87	99
7	cis-Hex-3-en-1-ol	–	328	13	88
8		–	358	30 (2 h)	99
9		–	393	81 (1.5 h)	99
10	trans-Hex-2-en-1-ol	CH ₂ Cl ₂	328	69	100
11		–	358	100 (6 h)	99
12		–	393	100 (10 min)	99
13	Geraniol	CH ₂ Cl ₂	328	58	100
14		–	358	100 (6 h)	100
15		–	393	100 (1.5 h)	100
16	R(+)-Limonene	CH ₂ Cl ₂	328	60	50 (39)
17		–	358	92 (1 h)	35 (61) ^d
18		–	393	99 (10 min)	17 (83) ^d
19	R(+)-Limonene	CH ₂ Cl ₂	328	94	73
20		–	358	61 (2 h)	100
21		–	393	98 (10 min)	100

^a All reactions carried out in the presence of 200 mol% oxidant and 1 mol% of molybdenum catalyst.

^b Calculated after 24 h, unless otherwise stated.

^c Calculated as "yield of epoxide"/"conversion" × 100% after 24 h.

^d Values in parentheses refer to di-epoxide yield.

The oxidation of R(+)-limonene followed the same trend as trans-hex-2-en-1-ol, with low substrate conversion (below 50%) for all catalysts, complex **1** being the best (60%). The two materials with the allyl ligand (**MCM-Pr-1** and **MCM-L₁-1**) showed higher conversions. All catalysts yielded the endocyclic epoxide as the major product with selectivity above 50%. Complex **1** shows the highest conversion and the lowest selectivity (Table 4, entry 31). Remarkably this catalyst also yields the di-epoxide (in both endo- and exo-cyclic positions) with 39% selectivity.

Complexes **1** and **2** display very high conversions in the oxidation of geraniol, but they become lower in the heterogeneous catalyst (Table 4, entries 37–42). The selectivities, however, are not very good. **1**, **MCM-Pr-2**, **MCM-L₁-1** and **MCM-L₁-2** yield geraniol-2,3-epoxide as the major product (shown in Table 2) with selectivity ranging from 62% to 87%. The by-product is geranial (all-trans product). **MCM-Pr-1** converts geraniol into the 6,7-epoxide (major product with 64% selectivity and 52% conversion), while complex **2** results in a ~1:1 ratio of both epoxides.

The catalysts were not very active, since conversions only exceeded 90% in very few examples. Cis-cyclooctene and cis-hex-3-en-1-ol were the only substrates selectively epoxidized (100%) by all catalysts. Only the catalysts containing **1** have the same performance in the oxidation of trans-hex-2-en-1-ol, the others leading to other products.

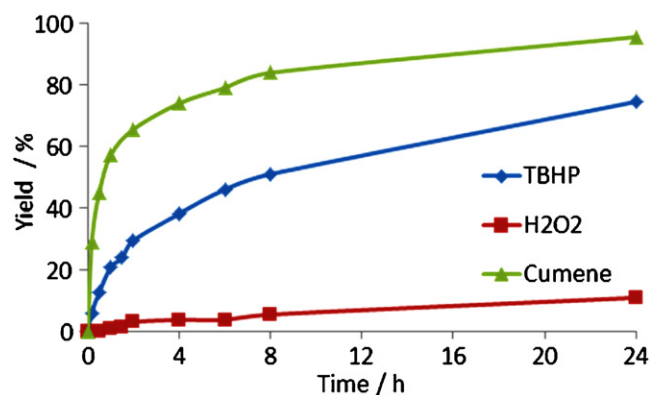
Table 6
cis-Cyclooctene epoxidation catalyzed by $[\text{Mo}(\eta^3\text{-C}_3\text{H}_5)\text{Br}(\text{CO})_2(\mathbf{8}\text{-aq})]$ (**1**) in CH₂Cl₂ with different oxidants.

Oxidant	Temperature (K)	Conversion ^{a,b} (%)	Selectivity ^{b,c} (%)
TBHP	328	74	100
TBHP	333	77	100
TBHP	338	86	100
H ₂ O ₂	328	11	100
CHP	328	95	100
CHP	333	100	100
CHP	338	97	100

^a All reactions carried out in CH₂Cl₂ in the presence of oxidant (200 mol%) and 1 mol% of molybdenum catalyst.

^b Calculated after 24 h, unless otherwise stated.

^c Calculated as "Yield of Epoxide"/"Conversion" × 100% after 24 h.

**Fig. 6.** cis-Cyclooctene epoxidation promoted by $[\text{Mo}(\eta^3\text{-C}_3\text{H}_5)\text{Br}(\text{CO})_2(\mathbf{8}\text{-aq})]$ (**1**) in CH₂Cl₂ at 328 K with different oxidants. All reactions carried out in the presence of oxidant (200 mol%) and 1 mol% of molybdenum catalyst.

Epoxidation of R(+)-limonene and geraniol occurred with fair to good substrate conversion, and mixtures of 2,3- and 6,7-epoxides were obtained. The major products were the endocyclic epoxide (limonene) and the 2,3-epoxide (geraniol). The diepoxide was also obtained in the oxidation of limonene (entry 31) and geraniol in

Table 7
cis-Cyclooctene epoxidation catalyzed by $[\text{Mo}(\eta^3\text{-C}_3\text{H}_5)\text{Br}(\text{CO})_2(\mathbf{8}\text{-aq})]$ (**1**) in CH₂Cl₂ at 328 K with variable oxidant:substrate ratio.

Oxidant	Ratio	Conversion ^{a,b} (%)	Selectivity ^{b,c} (%)
TBHP	1.00	92	100
TBHP	1.25	97	100
TBHP	1.50	99	100
TBHP	1.75	100	100
TBHP	2.00	74	100
CHP	1.00	77	100
CHP	1.50	94/88/74 ^d	100
CHP	2.00	95	100

^a All reactions carried out in CH₂Cl₂ in the presence of oxidant and 1 mol% of molybdenum catalyst at 328 K.

^b Calculated after 24 h reaction.

^c Calculated as "Yield of Epoxide"/"Conversion" × 100% after 24 h.

^d Values refer to 1st, 2nd and 3rd recycling runs.

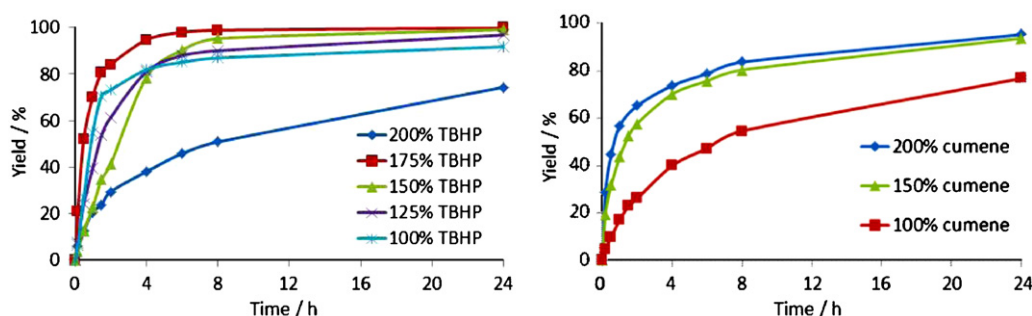


Fig. 7. *cis*-Cyclooctene epoxidation promoted by $[\text{Mo}(\eta^3\text{-C}_3\text{H}_5)\text{Br}(\text{CO})_2(\mathbf{8}\text{-aq})]$ (**1**) in CH_2Cl_2 at 328 K with variable oxidant:substrate ratio using as oxidant TBHP (left) and CHP (right). All reactions carried out in the presence of 1 mol% of molybdenum catalyst.

the oxidation of geraniol with selectivity up to 30% for both. Oxidation of styrene led to benzaldehyde as major product, arising from oxidative cleavage of the epoxide, but at shorter (8 h) reaction times, epoxide is generally the major product. The worst results were found in the oxidation of 1-octene, which was not achieved by any of the six catalysts.

In general the homogeneous catalysts performed better than the heterogeneous ones and systems containing the $\text{MoBr}(\eta^3\text{-C}_3\text{H}_5)(\text{CO})_2$ fragment (**1**, **MCM-Pr-1**, **MCM-L1-1**) better than the others.

3.2.2. The influence of reaction conditions and catalyst recycling

In an attempt to improve the conversion and selectivity in the oxidation of the substrates studied, the effect of solvent, temperature and oxidant were tested using complex $[\text{Mo}(\eta^3\text{-C}_3\text{H}_5)\text{Br}(\text{CO})_2(\mathbf{8}\text{-aq})]$ (**1**) as catalyst precursor, since it was the most promising one. Styrene was not considered in this study.

From the results in Table 5, it is obvious that reactions in CH_2Cl_2 at 328 K lead to low substrate conversions. In order to increase the temperature, solvents with higher boiling points, such as CH_3CN and toluene, were tried. The other possibility was to use the substrate as solvent, which allowed higher temperatures and higher concentration.

The most spectacular effect is observed in the oxidation of 1-octene. Three different solvents were tested (Table 5, entries 4–6) and the substrate conversion raises from 5 to 30 and 87% when moving from CH_2Cl_2 (328 K) to CH_3CN (358 K) and toluene (393 K). The selectivity toward the epoxide does not rise so much, but reaches 99% in toluene. Entries 7–9 show that increasing the temperature without adding solvent has the same effect both in conversion and selectivity, but the time to achieve the same conversion drops significantly. For instance, when the temperature

is raised to 358 K, the substrate conversion reaches 30% after 2 h reaction; at 393 K, conversion is 81% after 1.5 h.

This is an outstanding result since this is a non activated terminal olefin in a solvent free, greener process.

The same solventless conditions were tested for the other olefins (Table 5) and the same trend holds. Indeed, without added solvent and at 393 K, after 10 min all reactions become almost complete and epoxide selectivity reaches 100% for the majority of substrates (only *cis*-hex-3-en-1-ol requires 1.5 h, entry 15). The only exception in this seems to be *R*-(+)-limonene for which formation of the di-epoxide product is favored with increasing temperature. This can be seen as an important achievement since both limonene epoxide and di-epoxide products are industrially relevant in the production of low odor products such as metal coatings, varnishes, printing inks and UV curing applications.

Complex $[\text{Mo}(\eta^3\text{-C}_3\text{H}_5)\text{Br}(\text{CO})_2(\mathbf{8}\text{-aq})]$ (**1**) was also benchmarked as catalyst precursor in the epoxidation of *cis*-cyclooctene using three oxidants, *tert*-butyl hydroperoxide (TBHP), hydrogen peroxide (H_2O_2) and cumene hydroperoxide (CHP). The catalytic reactions with TBHP and CHP were performed in CH_2Cl_2 at 328 K, 333 K and 338 K, and with H_2O_2 in acetonitrile at 328 K. In this case acetonitrile was chosen since the water formed as by-product of the reaction of H_2O_2 would lead to a bi-phasic system with CH_2Cl_2 . The results are summarized in Table 6.

H_2O_2 is the oxidant leading to the worst results, with only 11% substrate conversion, although epoxide selectivity is complete. In TBHP, yields range from 74% to 86% and selectivity is kept with increasing temperature. When the oxidant is CHP, conversions are frankly better, ~20% above those observed with TBHP. Indeed conversion is at least 95% and selectivity is always complete for the epoxide. It can be seen in Fig. 6 that in CHP reaction kinetics is faster than in TBHP. For instance, at 328 K, substrate conversion is

Table 8
Olefin oxidation catalyzed by **MCM-L1-1** with TBHP or CHP.

Entry	Olefin	Solvent	Oxidant	Temperature (K)	Conversion ^{a,b} (%)	Selectivity ^{b,c} (%)
1	<i>cis</i> -Ciclooctene	CH_2Cl_2	TBHP	328	48 (1st run) 16 (2nd run) 14 (3rd run) 6 (4th run)	
2	100 <i>cis</i> -Ciclooctene	–	TBHP	393	100 ^d (1st run) 100 (2nd run) 100 (3rd run) 100 (4th run)	
3	<i>cis</i> -ciclooctene	CH_2Cl_2	CHP	328	31	100
4	1-Octeno	Toluene	TBHP	393	44	97
5	1-Octeno	–	TBHP	393	53	83
6	<i>cis</i> -Hex-3-en-1ol	–	TBHP	393	57	100

^a All reactions carried out in the presence of 200 mol% oxidant and 1 mol% of molybdenum catalyst.

^b Calculated after 24 h, unless otherwise stated.

^c Calculated as "Yield of epoxide"/"Conversion" × 100% after 24 h.

^d Achieved after 2 h.

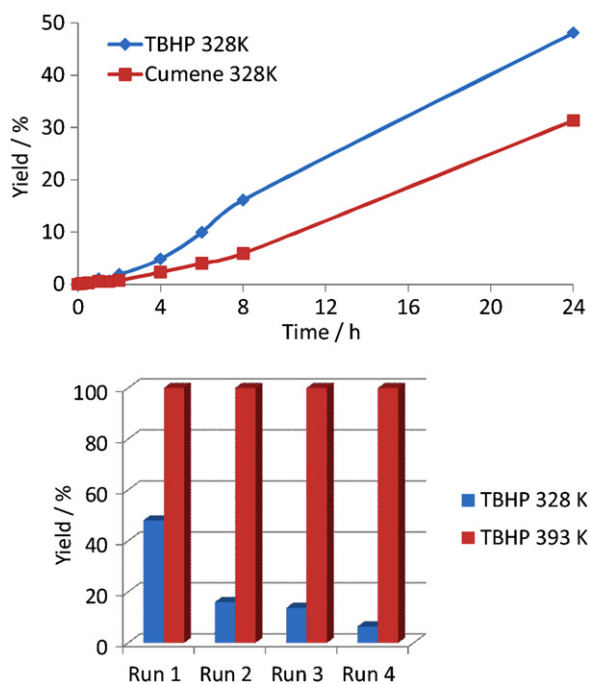


Fig. 8. *cis*-Cyclooctene epoxidation catalyzed by **MCM-L₁-1** in CH₂Cl₂ at 328 K with TBHP or CHP as oxidants (top). Recycling experiments of *cis*-cyclooctene epoxidation catalyzed by **MCM-L₁-1** with TBHP at 328 K in CH₂Cl₂, and at 393 K without solvent (bottom).

21% for TBHP and 57% for CHP after 1 h, accounting for the beneficial use of CHP. This shows that CHP is a better oxidant to be used with complex **1** as pre-catalyst for *cis*-cyclooctene epoxidation.

The oxidant:substrate ratio was also explored for the epoxidation of *cis*-cyclooctene in the presence of **1** in CH₂Cl₂ at 328 K, using either TBHP or CHP as oxidants. The oxidant:substrate ratio ranged between 1 and 2. The results are shown in Table 7 and Fig. 7.

With TBHP, substrate conversion increases slightly as the ratio goes from 100 to 175, but at a ratio of 2 significantly lower conversion and slower kinetics of the reaction are obtained (Fig. 7), indicating that possibly a large excess of the TBHP can slow down the reaction. This may be related to a large quantity of *t*-butanol formed as a by-product of TBHP reaction and its competition with TBHP for the catalysis leading to deactivation.

When the oxidant is CHP, the trends are different. Substrate conversion always increases with the increase of the oxidant:substrate ratio from 1 to 2 and this increase is rather large from 1 to 1.5. Recycling experiments conducted for the CHP oxidant with an oxidant:substrate ratio set at 1.5 indicate that the catalytic system shows recycling capability although it suffers from deactivation, as substrate conversion drops from 94% to 74% after the third cycle.

A similar study was performed using one heterogeneous catalyst containing complex **1**, **MCM-L₁-1**, three substrates (*cis*-cyclooctene, 1-octene, and *cis*-hex-3-en-1-ol), two oxidants (TBHP and CHP), and varying the solvent. The reutilization of the catalyst was also checked. All the results are collected in Table 8.

The epoxidation of *cis*-cyclooctene without added solvent at 393 K (Table 8, entry 2) results in a surprising performance compared to the standard conditions (Table 8, entry 1). In fact, 100% conversion is achieved after as little as 2 h in fresh use, while, on the other hand, the catalyst can be recycled without loss of activity for four cycles (calculated after 24 h). These results are outstanding compared to those reported in entry 1 of Table 8, and suggest that the solvent plays an important role in the catalyst deactivation. In fact, Mo elemental analysis reflected severe leaching during the first catalytic cycle, which certainly accounts for the loss of conversion

from 48 to 16% (Fig. 8 bottom). Nevertheless, at higher temperature but no added solvent, though leaching is likely to occur, the catalyst is able to adjust its performance although at the sake of slower kinetics. Epoxidation of *cis*-cyclooctene was also tested using CHP (Table 8, entry 3) as oxidant, but the performance was even lower than with TBHP under similar conditions (Fig. 8 top).

The same material was also used in the epoxidation of 1-octene (Table 6, entries 4 and 5) at temperatures higher than 328 K (Table 4, entry 17). The results are once again remarkable. From an almost inactive system at 328 K in CH₂Cl₂, the conversion increased from 4% to 44% in toluene at 393 K, while selectivity increased from 8% to excellent 97%. In the absence of added solvent, the conversion remains high at 393 K, but the selectivity drops. Nonetheless, these achievements demonstrate that 1-octene, a terminal linear olefin, which is therefore inactivated, requires more extreme conditions to suffer epoxidation.

Epoxidation of *cis*-hex-3-en-1-ol also benefits from running the experiments at higher temperature, since conversion increases from as little as 4% (Table 4, entry 29) to 57% (Table 8, last entry) keeping complete selectivity toward the epoxide.

4. Conclusions

The new Mo(II) complexes [MoBr(η³-C₃H₅)(CO)₂(8-aq)] (**1**) and [Mo₂(CO)₃(8-aq)] (**2**) were synthesized, characterized and immobilized in MCM-41, using a 3-iodopropyltrimethoxysilane spacer. Two procedures were adopted. In the first, the spacer reacted with the **8-aq** ligand forming **L₁**, which was directly supported in the material and then allowed to react with the parent complexes. In the second approach, the spacer was immobilized and reacted directly with complexes **1** and **2**. This last procedure was much less efficient in terms of metal load inside the material, although the functionalized materials were the same according to their characterization.

The complexes and the new materials were tested as the catalytic precursors in the epoxidation of several substrates, showing in most cases a high selectivity toward the epoxide, but usually low conversions, the best results being obtained by complex **1** (homogeneous conditions). Careful choice of conditions showed that the conversions could be improved up to a certain extent, by using the substrate as solvent and varying the oxidant:substrate ratio. TBHP seems the best oxidant to use with these catalysts. The materials exhibit in general a lower catalytic activity than the complexes (see Tables 4–6).

While we cannot rule out diffusion problems that may prevent the substrate from reaching active catalyst sites inside the pores, we believe that deactivation routes may involve the NH groups of the catalyst. Hydrogen bond networks may be formed with the catalyst, silanol groups still present in the material walls, and the oxidant (an alcohol). This effect has been observed before, but in the homogeneous catalyst only the NH groups and the alcohol interact in this way [27,29]. Interestingly, in the system where the heterogenized catalyst is more active than the homogeneous analogue there are no such groups present [25]. Recent studies, however, have shown that a number of molybdenum compounds, besides the active species, may result from the reaction of TBHP on analogues of complexes **1** and **2**, with 2,2'-bipyridine ligands. Such decomposition may also take place under milder catalytic conditions, contributing to a deactivation of the catalyst [43].

Acknowledgements

The authors thank FCT, POCI and FEDER (projects PTDC/QUI/71576/2006, PEst-OE/QUI/UI0612/2011, PEst-OE/QUI/UI0100/2011) for financial support. MSS (SFRH/BD/48640/2008) thanks FCT for a research grant.

References

- [1] M.H. Valkenberg, W.F. Hölderich, *Catal. Rev.* 44 (2002) 321–374.
- [2] A. Taguchi, F. Schüth, *Micropor. Mesopor. Mater.* 77 (2005) 1–45.
- [3] C.T. Kresge, M.E. Leonowicz, W.J. Roth, J.C. Vartuli, J.S. Beck, *Nature* 359 (1992) 710–712.
- [4] J.S. Beck, J.C. Vartuli, W.J. Roth, M.E. Leonowicz, C.T. Kresge, K.D. Schmitt, C.T.W. Chu, D.H. Olson, E.W. Sheppard, S.B. McCullen, J.B. Higgins, J.L. Schlenker, *J. Am. Chem. Soc.* 114 (1992) 10834–10843.
- [5] C.D. Nunes, M. Pillinger, A.A. Valente, I.S. Gonçalves, J. Rocha, P. Ferreira, F.E. Kühn, *Eur. J. Inorg. Chem.* (2002) 1100–1107.
- [6] T.A. Fernandes, C.D. Nunes, P.D. Vaz, M.J. Calhorda, P. Brandão, J. Rocha, I.S. Gonçalves, A.A. Valente, L.P. Ferreira, M. Godinho, P. Ferreira, *Micropor. Mesopor. Mater.* 112 (2008) 14–25.
- [7] J. Gimenez, C.D. Nunes, P.D. Vaz, A.A. Valente, P. Ferreira, M.J. Calhorda, *J. Mol. Catal. A* 256 (2006) 90–98.
- [8] C.D. Nunes, A.A. Valente, M. Pillinger, A.C. Fernandes, C.C. Romão, J. Rocha, I.S. Gonçalves, *J. Mater. Chem.* 12 (2002) 1735–1742.
- [9] D.M. Ford, E.E. Simanek, D.F. Shantz, *Nanotechnology* 16 (2005) S458–S475.
- [10] M. Pillinger, C.D. Nunes, P.D. Vaz, A.A. Valente, I.S. Gonçalves, P.J.A. Ribeiro-Claro, J. Rocha, L.D. Carlos, F.E. Kühn, *Phys. Chem. Chem. Phys.* 4 (2002) 3098–3105.
- [11] P. Oliveira, A. Machado, A.M. Ramos, I. Fonseca, F.M. Braz Fernandes, A.M. Botelho do Rego, J. Vital, *Micropor. Mesopor. Mater.* 120 (2009) 432–440.
- [12] R.G. Hayter, *J. Organomet. Chem.* 13 (1968) P1–P3.
- [13] H. tom Dieck, H. Friedel, *J. Organomet. Chem.* 14 (1968) 375–385.
- [14] P.K. Baker, M.B. Hursthouse, A.I. Karaulov, A.J. Lavery, K.M.A. Malik, D.J. Muldoon, A. Shawcross, *J. Chem. Soc., Dalton Trans.* (1994) 3493–3498.
- [15] (a) Y. Yamaguchi, K. Ogata, K. Kobayashi, T. Ito, *Dalton Trans.* (2004) 3982–3990; (b) P.K. Baker, *Adv. Organomet. Chem.* 40 (1996) 45–115.
- [16] (a) B.M. Trost, M. Lautens, *J. Am. Chem. Soc.* 104 (1982) 5543–5545; (b) B.M. Trost, M. Lautens, *J. Am. Chem. Soc.* 109 (1987) 1469–1478; (c) B.M. Trost, C.A. Merlic, *J. Am. Chem. Soc.* 112 (1990) 9590–9600.
- [17] D. Morales, J. Pérez, L. Riera, V. Riera, R. Corzo-Suárez, S. García-Granda, D. Miguel, *Organometallics* 21 (2002) 1540–1545.
- [18] V.S. Joshi, M. Nandi, H. Zhang, B.S. Haggerty, A. Sarkar, *Inorg. Chem.* 32 (1993) 1301–1303.
- [19] J.C. Alonso, P. Neves, M.J. Pires da Silva, S. Quintal, P.D. Vaz, C. Silva, A.A. Valente, P. Ferreira, M.J. Calhorda, V. Félix, M.G.B. Drew, *Organometallics* 26 (2007) 5548–5556.
- [20] A. Al-Ajlouni, D. Veljanovski, A. Capapé, J. Zhao, E. Herdtweck, M.J. Calhorda, F.E. Kühn, *Organometallics* 28 (2009) 639–645.
- [21] (a) J.-M. Brégeault, *Dalton Trans.* (2003) 3289–3302; (b) K.A. Jørgensen, *Chem. Rev.* 89 (1989) 431–458.
- [22] A. Sakthivel, J. Zhao, G. Raudaschl-Sieber, M. Hanzlik, A.S.T. Chiang, F.E. Kühn, *Appl. Catal. A: Gen.* 281 (2005) 267–273.
- [23] A.J. Burke, *Coord. Chem. Rev.* 252 (2008) 170–175.
- [24] M.S. Saraiva, S. Quintal, F.C.M. Portugal, T.A. Lopes, V. Félix, J.M.F. Nogueira, M. Meireles, M.G.B. Drew, M.J. Calhorda, *J. Organomet. Chem.* 693 (2008) 3411–3418.
- [25] M. Vasconcelos-Dias, C.D. Nunes, P.D. Vaz, P. Ferreira, P. Brandão, V. Félix, M.J. Calhorda, *J. Catal.* 256 (2008) 301–311.
- [26] M.S. Saraiva, N.L. Dias Filho, C.D. Nunes, P.D. Vaz, T.G. Nunes, M.J. Calhorda, *Micropor. Mesopor. Mater.* 117 (2009) 670–677.
- [27] M.S. Saraiva, C.D. Nunes, T.G. Nunes, M.J. Calhorda, *J. Mol. Catal. A* 321 (2010) 92–100.
- [28] M. Vasconcelos-Dias, S.R.M.M. de Aguiar, C.D. Nunes, P.D. Vaz, T.G. Nunes, M.J. Calhorda, *Curr. Inorg. Chem.* 1 (2011) 146–155.
- [29] N.L.D. Filho, F.C.M. Portugal, J.M.F. Nogueira, P. Brandão, V. Félix, P.D. Vaz, C.D. Nunes, M.J. Calhorda, *Organometallics* 31 (2012) 4495–4503.
- [30] C.I. Fernandes, N.U. Silva, P.D. Vaz, T.G. Nunes, C.D. Nunes, *Appl. Catal. A: Gen.* 384 (2010) 84–93.
- [31] (a) M.L. Clarke, D.J. Cole-Hamilton, D.F. Foster, A.M.Z. Slawin, J.D. Woollins, *J. Chem. Soc., Dalton Trans.* (2002) 1618–1624; (b) G. Brancatelli, D. Drommi, G. Feminó, M. Saporita, G. Bottari, F. Faraone, *New J. Chem.* 34 (2010) 2853–2860; (c) D. Shabashov, O. Daugulis, *J. Am. Chem. Soc.* 132 (2010) 3965–3972.
- [32] M. Kruk, M. Jaroniec, *Langmuir* 13 (1997) 6267–6273.
- [33] M. Kruk, V. Antochshuk, M. Jaroniec, *J. Phys. Chem. B* 103 (1999) 10670–10683.
- [34] J.R. Ascenso, C.G. de Azevedo, M.J. Calhorda, M.A.A.F. de, C.T. Carrondo, P. Costa, A.R. Dias, M.G.B. Drew, A.M. Galvão, C.C. Romão, V. Félix, *J. Organomet. Chem.* 632 (2001) 197–208.
- [35] P.M.F.J. Costa, M. Mora, M.J. Calhorda, V. Félix, P. Ferreira, M.G.B. Drew, H. Wadepohl, *J. Organomet. Chem.* 687 (2003) 57–68.
- [36] B. Marler, U. Oberhagemann, S. Voltmann, H. Gies, *Micropor. Mater.* 6 (1996) 375–383.
- [37] W. Hammond, E. Prouzet, S.D. Mahanti, T.J. Pinnavaia, *Micropor. Mesopor. Mater.* 27 (1999) 19–25.
- [38] S.J. Gregg, K.S.W. Sing, *Adsorption Surface Area and Porosity*, 2nd ed., Academic Press, London, 1982.
- [39] M.D. Alba, A. Becerro, J. Klinowski, *J. Chem. Soc., Faraday Trans.* 92 (1996) 849–854.
- [40] A.A. Romero, M.D. Alba, W. Zhou, J. Klinowski, *J. Phys. Chem. B* 101 (1997) 5294–5300.
- [41] M. Kruk, M. Jaroniec, *Langmuir* 15 (1999) 5410–5413.
- [42] P. Ferreira, C.D. Nunes, P.D. Vaz, N. Bion, P. Brandão, J. Rocha, *Prog. Solid State Chem.* 33 (2005) 163–170.
- [43] C.A. Gamelas, A.C. Gomes, S.M. Bruno, F.A.A. Paz, A.A. Valente, M. Pillinger, C.C. Romão, I.S. Gonçalves, *Dalton Trans.* 41 (2012) 3474–3484.